Zeeman-driven parity transitions in an Andreev quantum dot

A. M. Whiticar,[1,*] A. Fornieri,[1] A. Banerjee,[1] A. C. C. Drachmann,[1] S. Gronin,[2,3] G. C. Gardner,[2,3]
T. Lindemann,[2,3,4,5] M. J. Manfra,[2,3,4,5] and C. M. Marcus[1,†]

[1]*Center for Quantum Devices, Niels Bohr Institute, University of Copenhagen and Microsoft Quantum Lab–Copenhagen,
Universitetsparken 5, 2100 Copenhagen, Denmark*
[2]*Department of Physics and Astronomy and Microsoft Quantum Lab–Purdue, Purdue University, West Lafayette, Indiana 47907, USA*
[3]*Birck Nanotechnology Center, Purdue University, West Lafayette, Indiana 47907, USA*
[4]*School of Materials Engineering, Purdue University, West Lafayette, Indiana 47907, USA*
[5]*School of Electrical and Computer Engineering, Purdue University, West Lafayette, Indiana 47907, USA*

The Andreev spectrum of a quantum dot embedded in a hybrid semiconductor-superconductor interferometer
can be modulated by electrostatic gating, magnetic flux through the interferometer, and Zeeman splitting from
an in-plane magnetic field. We demonstrate parity transitions in the embedded quantum dot system and show
that the Zeeman-driven transition is accompanied by a 0-π transition in the superconducting phase across the
dot. We further demonstrate that flux through the interferometer modulates both dot parity and 0-π transitions.

I. INTRODUCTION

The interplay of confinement, spin, and superconductivity
leads to a rich variety of mesoscopic phenomena [1–3] that
can be investigated in semiconductor-superconductor hybrid
materials coupled via the proximity effect [3,4]. Recent advances in epitaxial growth of such hybrids have demonstrated
highly transparent heterointerfaces in several material platforms [5–8].

An important application is semiconducting Josephson
junctions (JJs), where a semiconducting normal (N) region
is bounded by two superconductors (S), giving rise to a
spectrum of Andreev bound states (ABSs) in the N region
at energies below the gap Δ of the superconductors [9].
ABS energies E depend on the superconducting phase difference φ across the junction and generate a supercurrent,
$I_s(\varphi) = -(2e/h)\,dE/d\varphi$, where e is the unit of charge and h
is Planck's constant [10,11]. Semiconducting S-N-S junctions
have been used as voltage-controlled transmons (gatemons)
[12–16] and Andreev qubits [17–20].

A quantum dot (QD) embedded in a Josephson junction (S-
QD-S) can result in a competition between superconductivity
and spin in a confined system [2,21–24]. The charging energy
of a weakly coupled QD typically stabilizes one of two spin
states at zero magnetic field, depending on dot occupancy:
a spin-zero singlet $|S\rangle$ or a spin-$\frac{1}{2}$ doublet $|D\rangle$ [23,25,26].
For even dot occupancy, the ground state (GS) is typically
a singlet for all coupling strengths; for odd occupancy, the
GS is either a $|D\rangle$ state for weak coupling or a delocalized
singlet, where the spin of the dot is hybridized with spins

in the leads [25]. The hybridized odd-parity subgap spectrum corresponds to Yu-Shiba-Rusinov states [25,27,28], and
the crossover between even and odd parity [23,26,29,30] is
marked by a zero-energy crossing [27,31–33].

Bound-state (BS) excitations at energies E_{BS} correspond
to the differences between GS and first excited-state (ES)
energies [32]. When $E_{\mathrm{BS}} = 0$, the GS and ES are degenerate, and a fermionic parity transition occurs [25,29]. The
even and odd GS parities can be distinguished by the phase
dependence of E_{BS}. An odd GS leads to a superconducting phase difference of π across the JJ, shifting the phase
dependence of the subgap excitations by π, which results
in a negative supercurrent [30,34]. The GS parity transition
from even to odd is commonly referred to as a 0-π phase
transition and can be identified spectroscopically by the observation of zero-bias crossings (ZBCs) and π-shifted phase
dependence of the subgap spectrum via tunneling of single
electrons into the junction from a weakly coupled normal lead
[23,29,31,35].

In this paper, we investigate an S-QD-S junction embedded
in a superconducting quantum interference device (SQUID).
The device allowed control of the superconducting phase
across the QD by threading magnetic flux through the SQUID
loop, while BS energies were simultaneously measured via
tunneling spectroscopy into the QD with a third (normal)
lead. The system was fabricated from an epitaxial InAs-Al
heterostructure patterned using electrostatic gates. We investigate spectra of subgap excitations under the influence of flux
and Zeeman field across parity transitions identified by ZBCs.
We observe that the subgap spectrum acquires a π-shifted
energy dependence in the odd-parity GS, as expected for a 0-π
phase transition. We find that these transitions are controlled
via magnetic field, gate voltage, and superconducting phase
difference, which demonstrates precise control of Andreev
states in semiconductor Josephson junctions.

*Present address: D-Wave Systems, Burnaby, British Columbia,
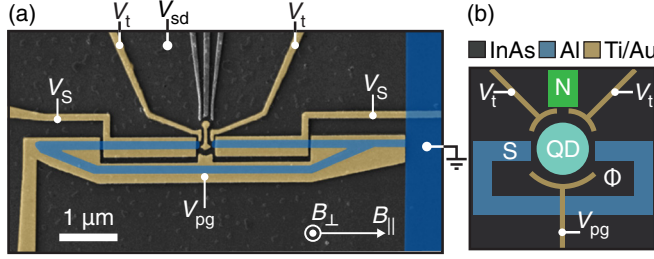Canada V5G 4M9.
†marcus@nbi.ku.dk

FIG. 1. (a) False-color electron micrograph of an S-QD-S device and (b) device schematic. The device consists of a loop (blue) of epitaxial Al and Ti/Au electrostatic gates (yellow). The junction is formed by two Al leads defined by gate voltage V_S and confined to a quantum dot (QD) by gate voltage V_{pg}. The tunnel barriers to the normal (N) lead and superconducting leads are controlled by gate voltage V_t. The ac+dc bias voltage V_{sd} is applied to the normal lead with the superconducting loop grounded. Magnetic field directions $B_\parallel$ and $B_\perp$ are shown, where $B_\perp$ is used to apply magnetic flux through the superconducting loop.

Magnetic-field-driven parity transitions in S-QD-S junctions have previously been observed as zeros of a reentrant critical current [36] or via direct spectroscopy of the QD [31,35]. Related measurements in N-QD-S devices showed gate voltage and field-driven parity transition as ZBCs [27,32]. Associated 0-π transitions were detected as supercurrent reversals when the S-QD-S junction was embedded in a SQUID [28,34,37,38]. In the present study, we spectroscopically interrogate the ABS spectrum of a S-QD-S junction, which reveals the ability of these parameters to work in concert with a superconducting phase difference to cause parity transitions.

II. DEVICE

Devices were fabricated from an InAs two-dimensional electron gas heterostructure grown on InP with 8 nm of epitaxial Al deposited *in situ*. Details of the heterostructure stack and device fabrication are given in Appendix A. Previous measurements on a similar material revealed near-unity transmission of the ABS in an S-N-S JJ [7,11].

We study two lithographically similar devices, A and B. Figure 1 shows a micrograph of device A. The superconducting loop was selectively wet etched from the Al film. A 15-nm HfO$_2$ dielectric layer, grown by atomic layer deposition, was then deposited over the entire device. Ti/Au top gates, patterned by electron-beam lithography, were then evaporated. The two S leads were defined by a negative gate voltage V_S, forming a ballistic JJ with a length of 200 nm and connected by an Al loop to form a single-junction SQUID. The QD between the two S leads was defined and controlled with a negative voltage V_{pg}. Typical QD charging energies varied between $U = 0.7$ and 1 meV, giving $U/\Delta \sim 4$ (see Fig. 10). Tunnel barriers to the N and S leads were controlled by gate voltage V_t applied to both barriers, providing tunneling spectroscopy of the S-QD-S junction. A voltage bias V_{sd} consisting of ac and dc components was applied to the normal semiconductor (N) lead, and the resulting current I and four-terminal voltage V_{4T} were measured using conventional
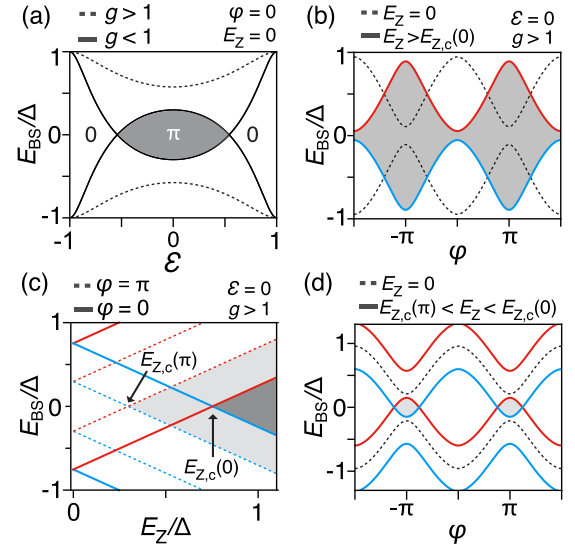

FIG. 2. Subgap excitation spectrum of an S-QD-S Josephson junction (JJ) as a function of detuning ε, centered on odd occupancy at $\varepsilon = 0$. (a) Bound-state energy $E_{BS}(\varepsilon)$ normalized by the gap Δ for strong ($g > 1$, dashed lines) and weak ($g < 1$, solid lines) coupling to the superconductors. The gray shaded region indicates the odd-parity ground state. (b) E_{BS} as a function of superconducting phase difference φ for an even-parity (dashed line) and odd-parity (solid line) ground state. (c) Dependence of E_{BS} on Zeeman energy $E_Z = |g^*|\mu_B B_\parallel$ for an even-parity ground state and for $\varphi = 0, \pi$ (solid and dashed lines, respectively). A ground-state parity transition, from even to odd parity, occurs when $E_{BS} = 0$ for a critical Zeeman energy $E_{Z,c}$. (d) $E_{BS}(\varphi)$ for an intermediate Zeeman energy [$E_{Z,c}(\pi) < E_Z < E_{Z,c}(0)$] where two zero-energy crossings occur near $\varphi = \pi$. Excitations are calculated based on a model introduced in Ref. [23] with an asymmetric lead coupling of $\theta \sim \pi/3$. Blue and red denote spin-resolved subgap states. Black denotes spin-degenerate states.

lock-in techniques with the S loop grounded. The in-plane magnetic fields $B_\parallel$ and perpendicular field $B_\perp$ were applied using a three-axis vector magnet. The superconducting phase difference φ across the junction was controlled by threading magnetic flux through the S loop, which has an area of 1.8 μm^2, so that ~ 1.2 mT corresponds to one flux quantum, $\Phi_0 = h/2e = 2.07$ mT μm^2.

III. MODEL

Before presenting experimental results, we first discuss the expected dependence of bound-state energies E_{BS} of the QD on level detuning ε, normalized Zeeman energy E_Z/Δ, and phase difference φ across the dot, including parity and 0-π transitions (see Appendix A 4 for further information). Detuning ε serves as a dimensionless gate voltage, defined such that $\varepsilon = 0$ is centered on an odd Coulomb valley, with $\varepsilon = \pm 1$ being the charge degeneracy points (see Appendix A 4). Figure 2(a) shows that for an odd-occupied QD, E_{BS} is lowered as ε is tuned away from ± 1. At the particle-hole symmetry point, $\varepsilon = 0$, the bound-state energy depends on the parameter g, which describes the exchange coupling strength

between the spin impurity and the S lead as [23,25]

$$E_{BS} = \Delta \frac{1 - g^2}{1 + g^2}. \tag{1}$$

For strong coupling [$g > 1$; dashed curves in Fig. 2(a)], E_{BS} does not reach zero for any value ε, preserving an even-parity GS. Physically, this is a consequence of strong screening of the unpaired spin of the QD by a quasiparticle in the S leads, which together form a delocalized singlet [25]. An increase in Coulomb interaction reduces g, which leads to a lowering of E_{BS}. For $g < 1$, E_{BS} crosses zero energy, signaling a transition to an odd GS parity within the shaded region of Fig. 2 [25].

The phase dependences of even- and odd-parity GSs are shown in Fig. 2(b). Dashed curves show the phase dependence for the even-parity GS (a zero junction, denoted 0-JJ), showing a 2π periodicity with E_{BS} minima at $\varphi = \pi$. For the odd-parity GS, the phase dependence acquires a π shift, with energy minima at $\varphi = 0$ (solid curves), yielding a π junction (denoted π-JJ). Notably, the 0-π transitions can be identified from this characteristic phase dependence of E_{BS}.

Zeeman coupling, for instance, from an in-plane magnetic field, can induce parity transitions by splitting an excited bound-state doublet by the Zeeman energy, $E_Z = |g^*|\mu_B B_\parallel$, giving $E_{BS}(B_\parallel) = E_{BS}(0) \pm E_Z/2$ [24,32,39], where g^* is the effective g factor and μ_B is the Bohr magneton [10,25,27,29]. In this scenario, at a critical Zeeman energy $E_{Z,c}$, a zero-energy crossing results in a transition to an odd-parity GS, as shown in Fig. 2(c) [27,32]. Increasing the magnetic field further reopens a gap that stabilizes a magnetic doublet GS with a π-shifted phase dispersion [40]. Note that Zeeman-induced parity transitions occur at reduced E_Z for nonzero φ [dashed curves in Fig. 2(c)].

Figure 2(d) shows the phase dependence of an even-parity GS for Zeeman coupling in the range $E_{Z,c}(\pi) < E_Z < E_{Z,c}(0)$. In this intermediate range, E_{BS} is lowered such that a gap opens in the vicinity of $\varphi = \pi$, marked by two zero-energy crossings, indicating an odd-parity GS. The size of the resulting gap increases with increasing Zeeman energy until E_Z reaches $E_{Z,c}(0)$, resulting in a dispersion with two minima, one at $\varphi = 0$ and one at $\varphi = \pi$, denoted 0′-JJ or π'-JJ, depending on which minimum is deeper [23,30].

IV. EXPERIMENT

A. Gate voltage dependence

Tunneling spectroscopy of the S-QD-S junction was performed by creating a tunnel barrier to the normal lead ($V_t = -1.87$ V). In Fig. 3(a), the differential conductance $G = dI/dV_{4T}$ is shown as a function of bias voltage V_{sd} and gate voltage V_{pg} used to tune the occupancy of the QD. When V_{pg} was varied, a gap of $V_{sd} \sim \pm 140\ \mu$V was observed, along with two subgap features. The first feature occurred at $V_{pg} \sim -5.74$ V [green marker in Fig. 3(a)], where the gap is reduced to $\sim 100\ \mu$V, indicating an odd QD occupancy with an even GS parity due to a strong coupling g [see dashed line in Fig. 2(a)].

At the stronger subgap feature in Fig. 3(a), around $V_{pg} \sim -5.85$ V, the gap closed entirely, resulting in two ZBCs, indicated by purple markers. Increasing V_t merged the ZBCs [black circle in Fig. 3(b)], then removed the
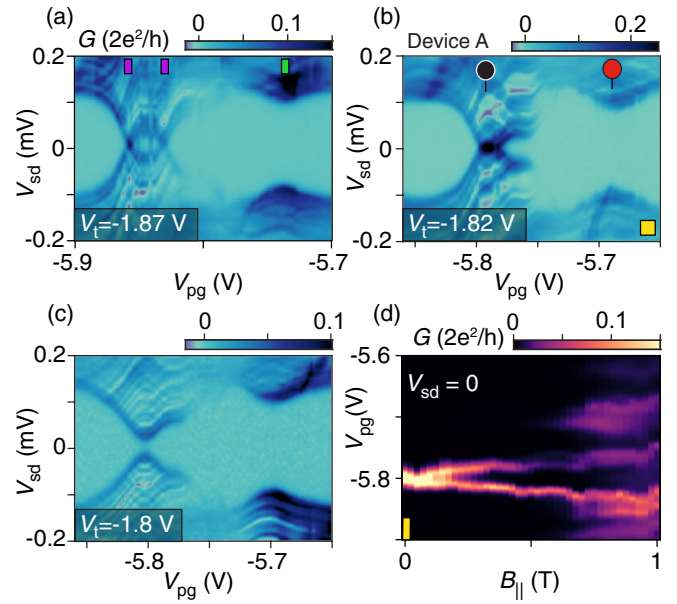

FIG. 3. Parity transition induced by voltage V_{pg} (device A). Differential conductance G as a function of bias V_{sd} and gate voltage V_{pg} for (a) tunnel-barrier gate voltage $V_t = -1.87$ V, (b) -1.82 V, and (c) -1.8 V. (d) Zero-bias conductance G as a function of in-plane magnetic field $B_\parallel$ and V_{pg} for $V_t = -1.82\ V$. In (a)–(c), $B_\parallel = \varphi = 0$.

crossings entirely [Fig. 3(c)]. The sequence demonstrates a gate-voltage-induced GS parity transition of the type illustrated in Fig. 2(a), where g is controlled by gate voltage V_t. The position in V_{pg} of the two subgap features shifts with V_t due to cross coupling. Figure 3(d) shows the dependence of the ZBC on $B_\parallel$ at the merging point, $V_t = -1.82$ V. The splitting is roughly linear in $B_\parallel$, yielding an effective g factor $g^* \sim 5$.

B. Phase dependence

We next examine the phase dependence of the even-parity GS at the location of the red marker in Fig. 3(b) ($V_{pg} = -5.69$ V, $V_t = -1.82$ V) by measuring the differential conductance G as a function of φ and V_{sd}, as shown in Fig. 4(a). Tuning φ from 0 to 2π lowers E_{BS}, eventually inducing a ZBC at $\varphi = \pi$. Applying an in-plane field $B_\parallel$ caused a gap to open in the vicinity of $\varphi = \pi$, as shown in Fig. 4(b). This gap increased with $B_\parallel$, while the gap at $\varphi = 0$ decreased, as shown in Figs. 4(b)–4(d). Although the induced superconducting gap is suppressed at $B_\parallel = 0.8$ T [Fig. 4(d)], it is evident that the minimum E_{BS} occurs at $\varphi = 0$. We interpret the gap opening at $\varphi = \pi$ as indicating 0′-JJ behavior of the type illustrated in Fig. 2(d).

The position of the ZBC in both φ and $B_\parallel$ is captured by measuring $G(V_{sd} = 0)$, as shown in Fig. 4(e). Increasing the field causes the crossing at $\varphi = \pi$ to split and move towards $\varphi = 0$, as shown in Fig. 4(f). The splitting, roughly linear at low fields, yields a g factor $g^* \sim 5$, consistent with the value found from Fig. 3(d). Cuts in Fig. 4(f) at $B_\parallel = 0$ and 0.8 T show minima shifted by π, indicating a 0-π transition driven by $B_\parallel$.
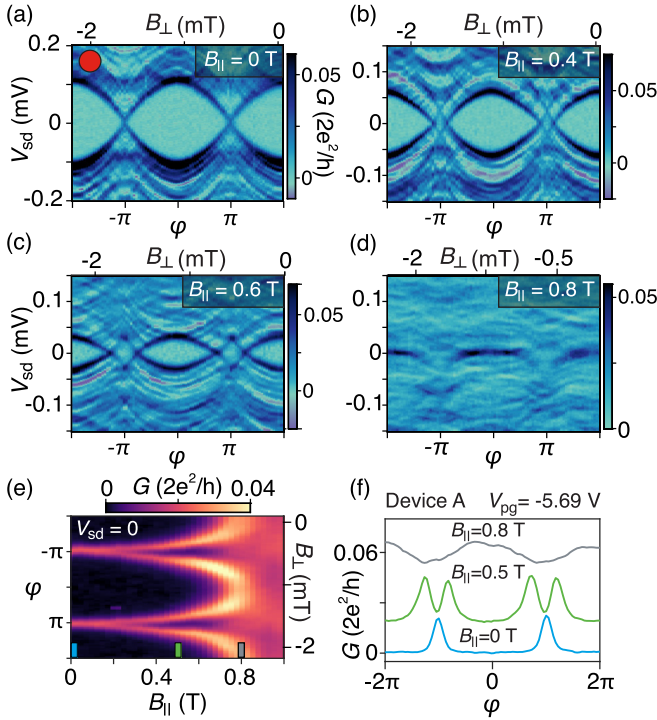
FIG. 4. Dependence of an even-parity ground state on the superconducting phase difference φ (device A). (a) Differential conductance G as a function of φ and bias voltage V_{sd} for in-plane magnetic field (a) $B_\parallel = 0$ T, (b) $B_\parallel = 0.4$ T, (c) $B_\parallel = 0.6$ T, and (d) $B_\parallel = 0.8$ T. (e) Zero-bias G as a function of φ and $B_\parallel$ with vertically offset linecuts shown in (f). The red marker indicates the V_{pg} position in Fig. 3 for reference.

Away from the feature marked by the red dot in Fig. 3(b), where the full gap is observed ($V_{pg} = -5.65$ V), ABSs do not cross zero bias at $\varphi = \pi$ at zero magnetic field (see Fig. 9).

C. Magnetic field dependence

We next investigate bound-state bias spectra as a continuous function of $B_\parallel$, rather than for the discrete values of $B_\parallel$ shown in Figs. 4(a)–4(d). Focusing now on device B, Fig. 5(a) shows a dip in E_{BS} as a function of gate voltage V_{pg} without ZBCs, measured at $B_\parallel = 0$. This indicates an even-parity GS and a doublet ES throughout this range of V_{pg}. Figure 5(b) shows that a ZBC is first observed for $B_\parallel \sim 0.5$ T at a phase difference of π. Increasing $B_\parallel$ further causes the ZBC to split and merge at $\varphi = 0$, similar to Fig. 4(e). Comparing the phase dependence of the ZBC between $B_\parallel = 0.5$ and 0.9 T, it is clear that the position of the ZBC in φ is π shifted, indicating a magnetic-field-induced 0-π transition. We attribute the finite field needed to induce a parity transition in device B in comparison to device A to reflect a different coupling g resulting from a different charging energy (see Fig. 8).

Figures 5(c)–5(e) show $E_{BS}(B_\parallel)$ for fixed φ. At $\varphi = \pi$ [Fig. 5(c)], E_{BS} splits from its zero-field value of $V_{sd} = \pm75$ μV, moving linearly towards zero, crossing zero bias at $B_\parallel = 0.6$ T, indicating a field-driven GS parity transition. At $\varphi = \pi/2$ [Fig. 5(d)] and $\varphi = 0$ [Fig. 5(e)] the larger zero-field splittings push the zero-bias crossing point to larger $B_\parallel$. A g
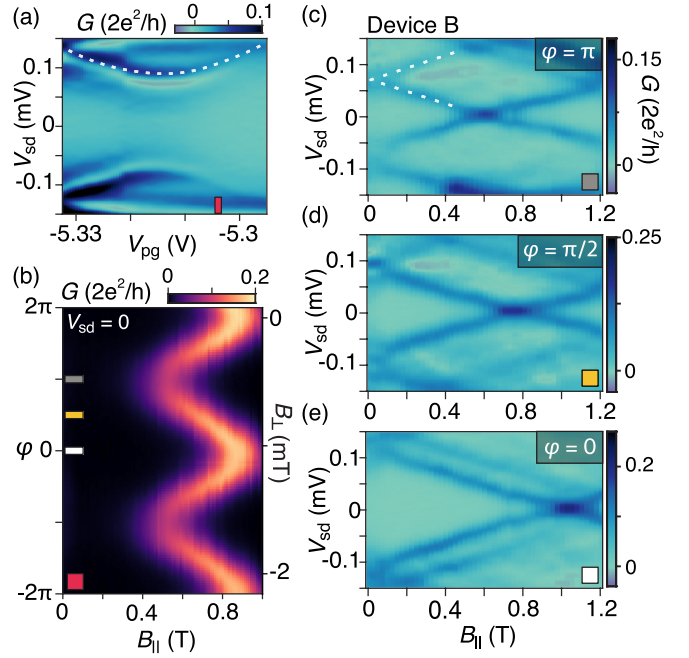

FIG. 5. Magnetic field dependence of an even-parity ground state (device B). (a) Differential conductance G as a function of gate voltage V_{pg} and bias voltage V_{sd} for $\varphi = B_\parallel = 0$. (b) Conductance G at zero bias as a function of φ and $B_\parallel$. G as a function of bias V_{sd} and in-plane field $B_\parallel$ for superconducting phase difference (c) $\varphi = \pi$, (d) $\pi/2$, and (e) 0. The plots in (c)–(e) are reconstructed from linecuts of Fig. 11 for fixed φ values. Dashed lines are guides to the eye.

factor $g^* \sim 4$, extracted from the slope of the lower ES, is insensitive to φ. The dependence of the zero-bias crossing field on φ is consistent with expectations in Fig. 2(c). Figure 11 shows the spectroscopy of $E_{BS}(\varphi)$ for fixed $B_\parallel$, displaying a continuous evolution of the 0-π transition.

D. Odd-parity ground state

The odd-parity transition indicated by the black marker in Fig. 3(b) is investigated in Fig. 6. At zero field, $E_{BS}(\varphi)$ is π shifted compared to the even-parity case (Fig. 4), with a minimum at $\varphi = 0$, indicating a π junction. Near the odd-parity transition, $E_{BS}(\varphi)$ shows a reduced dependence on φ,
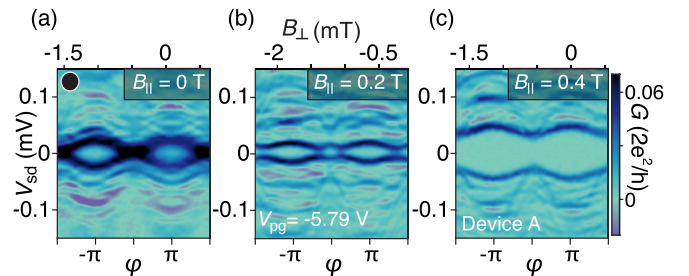

FIG. 6. Phase dependence of the odd-parity ground state (device A). Differential conductance G as a function of superconducting phase difference φ and bias V_{sd} for (a) $B_\parallel = 0$, (b) $B_\parallel = 0.2$ T, (c) $B_\parallel = 0.4$ T. The black marker indicates the V_{pg} position in Fig. 3 for reference.
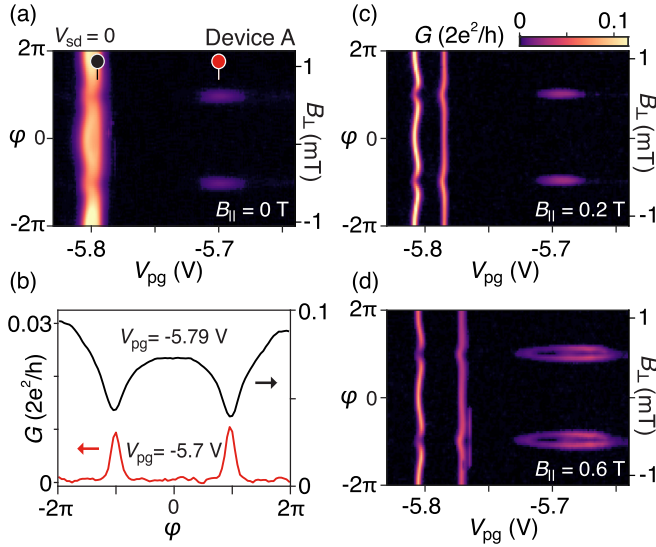
FIG. 7. Evolution of zero-bias crossings (device A). (a) Differential conductance G at zero bias as a function of phase difference φ and gate voltage V_{pg} for (a) $B_{\parallel} = 0$. Red and black markers show positions of linecuts in (b). Note the opposite behaviors along the two linecuts, as discussed in the text. (b) Linecuts of (a) for even-parity (red line) and odd-parity (black line) ground states. (c) Same as (a), but for $B_{\parallel} = 0.2$ T. (d) Same as (a), but for $B_{\parallel} = 0.6$ T.

as reported previously [31,35]. Increasing $B_{\parallel}$ increases E_{BS}, opening a gap for all φ that increases with field while retaining the π phase shift. This behavior is consistent with theory (see Fig. 2) [40].

E. Zero-bias crossings

The contribution of in-plane magnetic field, phase difference, and gate voltage on GS parity and 0-π transitions is identified by measuring $G(V_{pg}, \varphi)$ at zero bias in device A (see Fig. 7). This allows for the phase dependence of the ZBCs to be highlighted at specific V_{pg} values. Figure 7(a) shows two distinct values of V_{pg} where ZBCs occur at $B_{\parallel} = 0$ (see red and black markers).

At $V_{pg} = -5.7$ V, ZBCs are observed at $\varphi = \pi$, marking the position of the even-parity GS investigated in Fig. 4. We interpret the limited range of this ZBC in V_{pg} to reflect the energy dependence of $E_{BS}(\varepsilon)$ illustrated in Fig 2(a), with the red marker signifying $\varepsilon = 0$. For increasing magnetic field the ZBC at $\varphi = \pi$ splits in both φ and V_{pg}, stabilizing an odd-parity GS [see Fig. 7(d)].

For $V_{pg} = -5.8$ V, a bright vertical band is observed that indicates the odd-parity GS examined in Fig. 6. In Fig. 7(b) the phase dependence of the two GS locations is compared and reveals a π-shifted $E_{BS}(\varphi)$ dependence for the odd-parity GS. Increasing $B_{\parallel} = 0.2$ T causes the odd-occupancy ZBC to split in V_{pg} while retaining a π-shifted phase dependence with $g^* \sim 5$. The results of Fig. 7 reveals how the combination of gate voltage, magnetic field, and phase difference can control subgap excitations of the system and induce GS parity transitions.

V. CONCLUSION

To summarize, we have measured the subgap spectrum of an S-QD-S Josephson junction under the influence of gate voltage, in-plane magnetic field, and superconducting phase difference. We found that odd QD occupancies were not always accompanied by parity transitions or π-shifted Andreev spectrum. However, by controlling either the coupling, magnetic field, or phase difference, subgap excitations could be lowered to zero bias, inducing a parity transition. Furthermore, we showed that by applying a finite phase difference across the junction, parity transitions can occur at lower magnetic fields.

These results may have important implications for semiconductor-based superconducting qubits [14], which recently showed that an unintentional QD resonance resulted in a suppressed charge dispersion [15,16]. We demonstrated that highly tunable QDs can be intentionally placed in the weak link, which may enable an alternative mechanism for charge noise suppression while retaining large qubit anharmonicity. Moreover, these results introduce means of manipulating the spin of the ABS that could be used to control Andreev qubits [19,20].

Our results demonstrate both the high material quality and device design flexibility offered by the InAs-Al heterostructure material platform. The S-QD-S device design studied here is a promising candidate for investigating the hybridization of a QD with Majorana zero modes in the pursuit of parity readout of a topological qubit [41].

APPENDIX A

1. Wafer structure

The wafers used for fabricating the devices were grown by molecular beam epitaxy. The material stack consists of an InP substrate with a 100-nm-thick $In_{0.52}Al_{0.48}As$ lattice-matched buffer, a 1-μm-thick step-graded buffer realized with alloy steps from $In_{0.52}Al_{0.48}As$ to $In_{0.89}Al_{0.11}As$ (20 steps, 50 nm/step), a 58-nm $In_{0.82}Al_{0.18}As$ layer, a 4-nm $In_{0.75}Ga_{0.25}As$ bottom barrier, a 7-nm InAs quantum well, a 10-nm $In_{0.75}Ga_{0.25}As$ top barrier, two monolayers of GaAs, and a 7-nm film of epitaxial Al deposited *in situ* without breaking the MBE chamber vacuum.

Hall bar device geometries (where the Al was removed) were used to characterize the two-dimensional electron gas and revealed an electron mobility peak $\mu = 43\,000$ cm^2 V^{-1} s^{-1} for an electron density $n = 8 \times 10^{11}$ cm^{-2}, corresponding to an electron mean free path of $l_e \sim 600$ nm.

2. Fabrication details

Devices were fabricated using standard electron-beam lithography and wet-etching techniques. The devices were

electrically isolated using a two-step mesa etch by first removing the top Al film with Al etchant Transene D and then a deep ~300-nm III-V chemical wet etch $H_2O : C_6H_8O_7 : H_3PO_4 : H_2O_2$ (220:55:3:3). In a following lithography step, the Al film on the mesa was selectively etched into a SQUID with Al etchant Transene D at 50 °C. A 15-nm-thick layer of insulating HfO_2 was grown over the entire sample by atomic layer deposition at a temperature of 90 °C. Finally, top gates of Ti/Au (5/25 nm) were deposited by electron-beam evaporation and connected to bonding pads with leads of Ti/Au (5/300 nm).

3. Measurement details

Electrical measurements were performed in a dilution refrigerator at a base temperature of 20 mK. Using conventional lock-in techniques at 166 Hz, an ac excitation voltage of 3 μV and a variable dc bias voltage V_{sd} were applied to the normal lead Ohmic, as shown in Fig. 1. The resulting current across the device was recorded by grounding the superconducting loop Ohmic via a low-impedance current-to-voltage converter, and the four-terminal voltage was measured by an ac voltage amplifier with an input impedance of 500 MΩ.

4. Model details

The energy of the subgap excitations in an S-QD-S system was theoretically examined under the influence of QD level detuning $\varepsilon = 1 + 2\epsilon_d/U$, which serves as a dimensionless gate voltage that controls the QD level position ϵ_d, centered on an odd Coulomb valley, where U is the charging energy of the dot. Dependence on the coupling to the superconductor g, magnetic field $B_\parallel$, and superconducting phase difference φ follows the model investigated by Kiršanskas *et al.* [23]. This is an Anderson-type model describing a single Coulomb blockaded QD level coupled to two S leads with gaps $\Delta \exp(\pm i\varphi/2)$ in the limit of $U \gg \Delta$. The excitations in this model are Yu-Shiba-Rusinov states resulting from spinful odd QD occupancies.

In Fig. 2 we examine the energy of bound-state excitations E_{BS} in an S-QD-S JJ. The bound-state energies are calculated from [23]

$$E_{\pm,\sigma} = \frac{1}{2}\sigma E_Z - \frac{\sigma c_\pm \Delta}{\sqrt{(1+u)^2 + 4g^2}}[(1+u)(1+\chi u)$$
$$+ 2g^2 \pm 2g\sqrt{g^2 + u(1-\chi)(1+\chi u)}]^{1/2}, \quad \text{(A1)}$$

where the following shorthand notation is used:

$$\chi = 1 - \sin^2(2\theta)\sin^2(\phi/2), \quad u = w^2 - g^2, \quad c_+ = 1,$$
$$c_- = \text{sign}(1 + \chi u), \quad \tan(\theta) = t_R/t_L. \quad \text{(A2)}$$

The exchange scattering amplitude $g_{i,j} = \frac{4}{1-\varepsilon^2}\frac{t_i t_j}{U}$ and the potential scattering amplitude $w_{i,j} = \frac{2\varepsilon}{1-\varepsilon^2}\frac{t_i t_j}{U}$, with $g = g_{L,L} + g_{R,R}$ and $w = w_{L,L} + w_{R,R}$, both depend on the position of the detuning ε. The spin of the bound states $\sigma = \pm 1$ is either aligned or antialigned with respect to the spin of the QD. An angle θ is introduced to account for an asymmetry between the left and right tunnel barriers ($t_{R/L}$) to the superconducting leads, where $\theta = \pi/4$ represents a symmetrical coupling. In
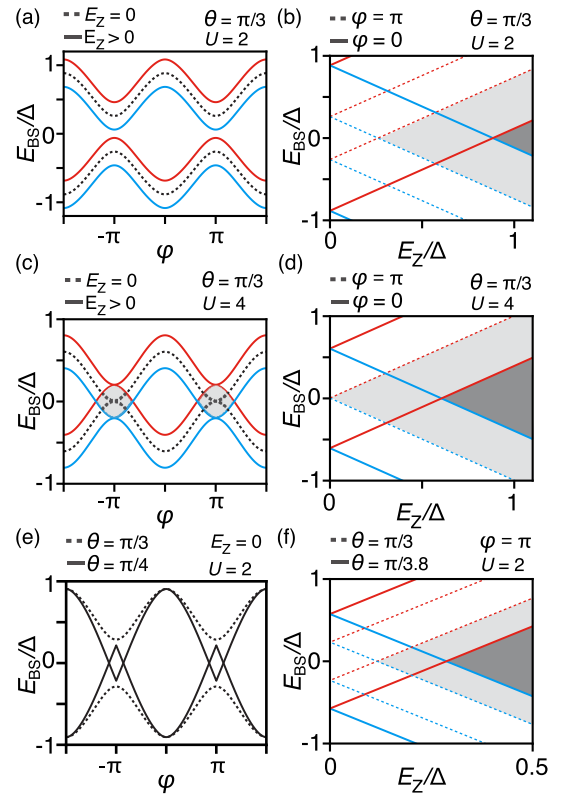

FIG. 8. Dependence of bound-state spectra on the superconducting phase difference φ and Zeeman energy E_Z for (a) and (b) charging energy $U = 2$ and (c) and (d) $U = 4$ for asymmetric coupling to the superconducting leads $\theta = \pi/3$. (e), (f) Dependence of asymmetric coupling φ on phase dispersion and the Zeeman energy of the bound-state excitations.

Ref. [23] these bound-state energies are used to calculate the conductance with a weakly coupled normal lead [similar setup as in Fig. 1(b)], where good agreement between the simulated conductance and the subgap spectra shown in Fig. 2 is found.

In Figs. 8(a)–8(d) the dependence of a varying charging energy U is shown. By decreasing the charging energy, a gap at $\varphi = \pi$ opens up due to an increased g. This shifts the critical Zeeman energy to higher fields [see Figs. 8(b) and 8(d)]. Figures 8(e) and 8(f) show the effect of coupling asymmetry on the phase dispersion. Asymmetric left/right coupling can open a gap at $\varphi = \pi$, which can be closed by symmetrizing the coupling or applying a magnetic field.

In the model of Kiršanskas *et al.* [23], a polarized spin approximation on the QD is employed to derive Eq. (A1). Therefore, the Zeeman energy does not influence the QD but induces spin splitting in the superconducting leads. Experimentally, we interpret the observed magnetic field dependence to reflect Zeeman splitting of the doublet ground states, as discussed theoretically in Refs. [25,27] and experimentally in Ref. [32]. Experimentally, it is challenging to differentiate between the two Zeeman splitting mechanisms since they contribute different g factor values, as discussed in Ref. [33]. We therefore assume an effective g factor g^* that accounts for a contribution from both mechanisms.
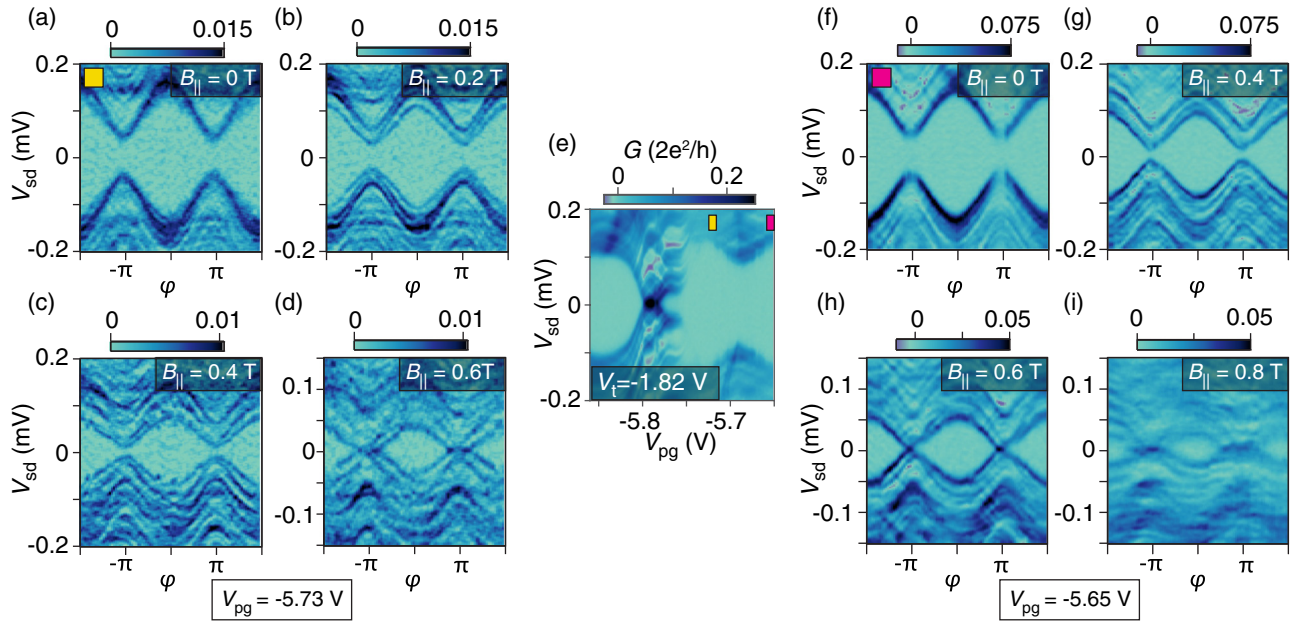
FIG. 9. Dependence of an even-parity ground state on a superconducting phase difference φ for intermediate values of V_{pg} in device A. (a)–(d) Differential conductance G as a function of φ and bias voltage V_{sd} for (a) magnetic field $B_{\parallel} = 0$, (b) 0.2, (c) 0.4, and (d) 0.6 T for $V_{pg} = -5.73$ V. (e) G as a function of V_{sd} and V_{pg} for tunnel barrier gate voltage $V_t = -1.82$ V. (f)–(i) G as a function of φ and V_{sd} for (f) $B_{\parallel} = 0$, (g) 0.4, (h) 0.6, and (i) 0.8 T for $V_{pg} = -5.65$ V.

APPENDIX B

In Fig. 9, phase dependence of an even parity ground state is shown for V_{pg} values on either side from the particle-hole symmetry point of $V_{pg} = -5.69$ V [see Fig. 2(a)]. At these two detuning points the subgap states no longer cross zero-bias at $\varphi = \pi$, while a magnetic field of $B_{\parallel} = 0.6$ T is able to induce a ZBC. We observe that the energy difference between $\varphi = \pi$ and 0 remains constant and only is shifted in energy due to the position of V_{pg}.

The normal state ($B_{\perp} > 200$ mT) Coulomb blockade for device A is shown in Fig. 10(a) and 10(c). We extract a charging energy from the Coulomb diamonds between 0.7 and 1 meV. In the superconducting state we observe a gapped spectrum with subgap states as discussed in the main text.

Figure 11 shows magnetic field increments of the phase dispersion in device B, which highlights the continuous evolution of the 0-π transition in both field and phase (see Fig. 5). For Fig. 11(a)–11(d) the subgap spectrum remains gapped for all φ values. At $B_{\parallel} = 0.5$ T a ZBC is observed at $\varphi = \pi$ and
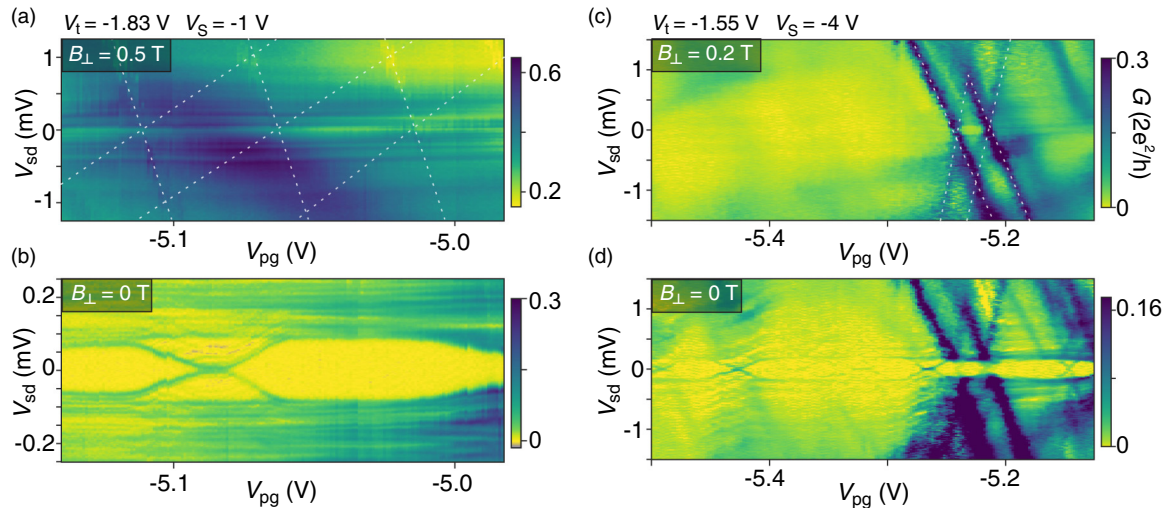

FIG. 10. Coulomb blockade in device A. (a)–(d) Differential conductance G as a function of bias voltage V_{sd} and V_{pg} (a) and (c) in the normal state and (b) and (d) in the superconducting state. (a) and (b) are measured in a gate configuration similar to that shown in Fig. 3(b). (c) and (d) are measured with more negative V_S gate voltages to allow for clearer Coulomb blockade features.
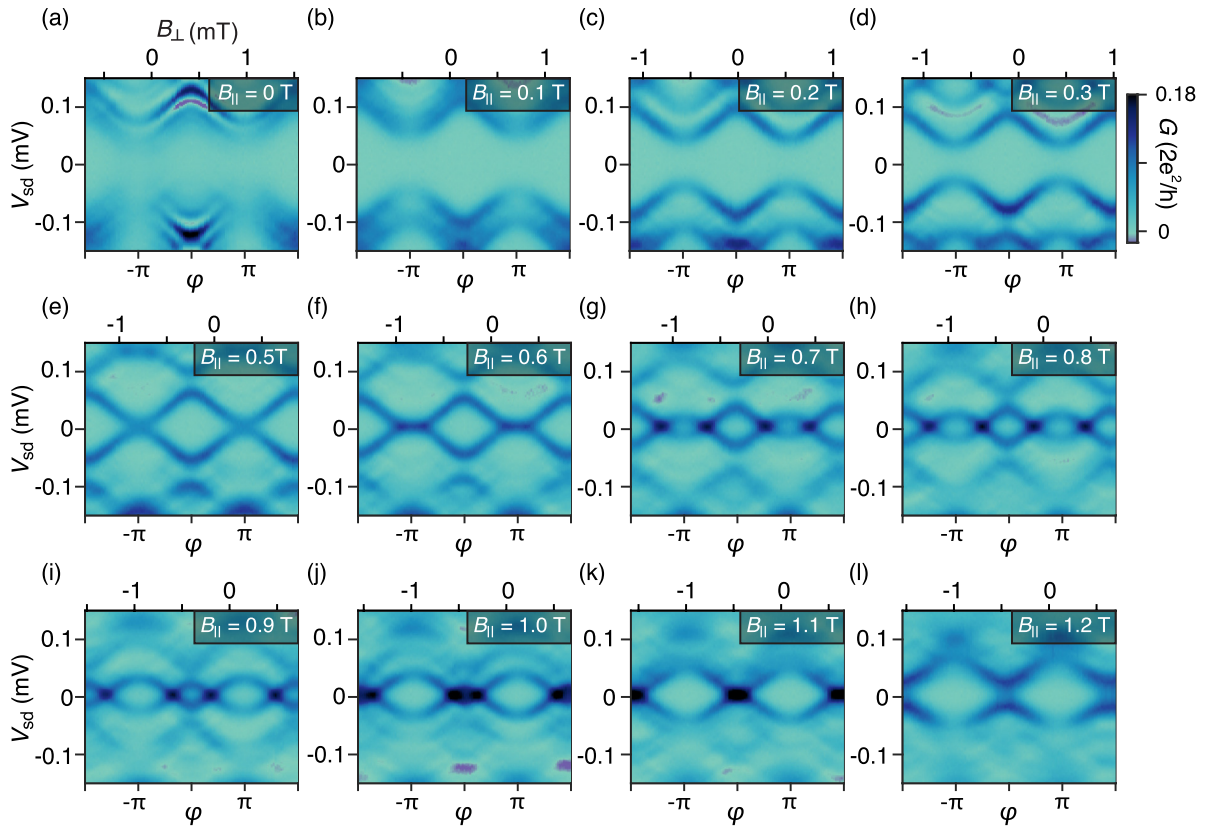
FIG. 11. Evolution of phase dispersion in magnetic field for device B. (a)–(l) Differential conductance G as a function of φ and bias voltage V_{sd} for increasing magnetic field $B_{\parallel}$.

as the magnetic field increases, the minima in φ transitioning from π to 0. Finally for $B_{\parallel} > 1.1$ T the subgap spectrum is again fully gapped for all φ values and the 0-π transition is complete.

[1] M. Eschrig, Phys. Today **64**(1), 43 (2011).

[2] S. De Franceschi, L. Kouwenhoven, C. Schönenberger, and W. Wernsdorfer, Nat. Nanotechnol. **5**, 703 (2010).

[3] T. Klapwijk, J. Supercond. **17**, 593 (2004).

[4] V. V. Ryazanov, V. A. Oboznov, A. Y. Rusanov, A. V. Veretennikov, A. A. Golubov, and J. Aarts, Phys. Rev. Lett. **86**, 2427 (2001).

[5] P. Krogstrup, N. Ziino, W. Chang, S. Albrecht, M. Madsen, E. Johnson, J. Nygård, C. Marcus, and T. Jespersen, Nat. Mater. **14**, 400 (2015).

[6] J. Shabani, M. Kjaergaard, H. J. Suominen, Y. Kim, F. Nichele, K. Pakrouski, T. Stankevic, R. M. Lutchyn, P. Krogstrup, R. Feidenhans'l, S. Kraemer, C. Nayak, M. Troyer, C. M. Marcus, and C. J. Palmstrøm, Phys. Rev. B **93**, 155402 (2016).

[7] M. Kjaergaard, H. J. Suominen, M. P. Nowak, A. R. Akhmerov, J. Shabani, C. J. Palmstrøm, F. Nichele, and C. M. Marcus, Phys. Rev. Applied **7**, 034029 (2017).

[8] R. M. Lutchyn, E. P. Bakkers, L. P. Kouwenhoven, P. Krogstrup, C. M. Marcus, and Y. Oreg, Nat. Rev. Mater. **3**, 52 (2018).

[9] C. W. J. Beenakker, Phys. Rev. Lett. **67**, 3836 (1991).

[10] T. Yokoyama, M. Eto, and Y. V. Nazarov, Phys. Rev. B **89**, 195407 (2014).

[11] F. Nichele, E. Portolés, A. Fornieri, A. M. Whiticar, A. C. C. Drachmann, S. Gronin, T. Wang, G. C. Gardner, C. Thomas, A. T. Hatke, M. J. Manfra, and C. M. Marcus, Phys. Rev. Lett. **124**, 226801 (2020).

[12] G. de Lange, B. van Heck, A. Bruno, D. J. van Woerkom, A. Geresdi, S. R. Plissard, E. P. A. M. Bakkers, A. R. Akhmerov, and L. DiCarlo, Phys. Rev. Lett. **115**, 127002 (2015).

[13] T. W. Larsen, K. D. Petersson, F. Kuemmeth, T. S. Jespersen, P. Krogstrup, J. Nygård, and C. M. Marcus, Phys. Rev. Lett. **115**, 127001 (2015).

[14] L. Casparis, M. R. Connolly, M. Kjaergaard, N. J. Pearson, A. Kringhøj, T. W. Larsen, F. Kuemmeth, T. Wang, C. Thomas, S. Gronin, G. C. Gardner, M. J. Manfra, C. M. Marcus, and K. D. Petersson, Nat. Nanotechnol. **13**, 915 (2018).

[15] A. Kringhøj, B. van Heck, T. W. Larsen, O. Erlandsson, D. Sabonis, P. Krogstrup, L. Casparis, K. D. Petersson, and C. M. Marcus, Phys. Rev. Lett. **124**, 246803 (2020).

[16] A. Bargerbos, W. Uilhoorn, C.-K. Yang, P. Krogstrup, L. P. Kouwenhoven, G. de Lange, B. van Heck, and A. Kou, Phys. Rev. Lett. **124**, 246802 (2020).

[17] A. Zazunov, V. S. Shumeiko, E. N. Bratus', J. Lantz, and G. Wendin, Phys. Rev. Lett. **90**, 087003 (2003).

[18] C. Janvier, L. Tosi, L. Bretheau, Ç. Ö Girit, M. Stern, P. Bertet, P. Joyez, D. Vion, D. Esteve, M. F. Goffman, H. Pothier, and C. Urbina, Science **349**, 1199 (2015).

[19] M. Hays, G. de Lange, K. Serniak, D. J. van Woerkom, D. Bouman, P. Krogstrup, J. Nygård, A. Geresdi, and M. H. Devoret, Phys. Rev. Lett. **121**, 047001 (2018).

[20] L. Tosi, C. Metzger, M. F. Goffman, C. Urbina, H. Pothier, S. Park, A. L. Yeyati, J. Nygård, and P. Krogstrup, Phys. Rev. X **9**, 011010 (2019).

[21] A. Eichler, M. Weiss, S. Oberholzer, C. Schönenberger, A. Levy Yeyati, J. C. Cuevas, and A. Martín-Rodero, Phys. Rev. Lett. **99**, 126602 (2007).

[22] T. Sand-Jespersen, J. Paaske, B. M. Andersen, K. Grove-Rasmussen, H. I. Jørgensen, M. Aagesen, C. B. Sørensen, P. E. Lindelof, K. Flensberg, and J. Nygård, Phys. Rev. Lett. **99**, 126603 (2007).

[23] G. Kiršanskas, M. Goldstein, K. Flensberg, L. I. Glazman, and J. Paaske, Phys. Rev. B **92**, 235422 (2015).

[24] J. He, D. Pan, G. Yang, M. Liu, J. Ying, Z. Lyu, J. Fan, X. Jing, G. Liu, B. Lu, D. E. Liu, J. Zhao, L. Lu, and F. Qu, Phys. Rev. B **102**, 075121 (2020).

[25] R. Žitko, J. S. Lim, R. López, and R. Aguado, Phys. Rev. B **91**, 045441 (2015).

[26] T. Meng, S. Florens, and P. Simon, Phys. Rev. B **79**, 224521 (2009).

[27] A. Jellinggaard, K. Grove-Rasmussen, M. H. Madsen, and J. Nygård, Phys. Rev. B **94**, 064520 (2016).

[28] R. Delagrange, R. Weil, A. Kasumov, M. Ferrier, H. Bouchiat, and R. Deblock, Phys. Rev. B **93**, 195437 (2016).

[29] E. Vecino, A. Martín-Rodero, and A. Levi Yeyati, Phys. Rev. B **68**, 035105 (2003).

[30] A. V. Rozhkov and D. P. Arovas, Phys. Rev. Lett. **82**, 2788 (1999).

[31] W. Chang, V. E. Manucharyan, T. S. Jespersen, J. Nygård, and C. M. Marcus, Phys. Rev. Lett. **110**, 217005 (2013).

[32] E. J. Lee, X. Jiang, M. Houzet, R. Aguado, C. M. Lieber, and S. De Franceschi, Nat. Nanotechnol. **9**, 79 (2014).

[33] W.-V. van Gerven Oei, D. Tanasković, and R. Žitko, Phys. Rev. B **95**, 085115 (2017).

[34] J. A. Van Dam, Y. V. Nazarov, E. P. Bakkers, S. De Franceschi, and L. P. Kouwenhoven, Nature (London) **442**, 667 (2006).

[35] J. Pillet, C. Quay, P. Morfin, C. Bena, A. L. Yeyati, and P. Joyez, Nat. Phys. **6**, 965 (2010).

[36] J. C. Estrada Saldaña, R. Žitko, J. P. Cleuziou, E. J. H. Lee, V. Zannier, D. Ercolani, L. Sorba, R. Aguado, and S. De Franceschi, Sci. Adv. **5**, eaav1235 (2019).

[37] C. Li, B. de Ronde, J. de Boer, J. Ridderbos, F. Zwanenburg, Y. Huang, A. Golubov, and A. Brinkman, Phys. Rev. Lett. **123**, 026802 (2019).

[38] D. Razmadze, E. C. T. O'Farrell, P. Krogstrup, and C. M. Marcus, Phys. Rev. Lett. **125**, 116803 (2020).

[39] V. Meden, J. Phys.: Condens. Matter **31**, 163001 (2019).

[40] N. Wentzell, S. Florens, T. Meng, V. Meden, and S. Andergassen, Phys. Rev. B **94**, 085151 (2016).

[41] T. Karzig, C. Knapp, R. M. Lutchyn, P. Bonderson, M. B. Hastings, C. Nayak, J. Alicea, K. Flensberg, S. Plugge, Y. Oreg, C. M. Marcus, and M. H. Freedman, Phys. Rev. B **95**, 235305 (2017).